ARTICLE OPEN

CDX2 downregulation regulates intrinsic WNT pathway activation, dictating metastasis in *APC* and *CTNNB1* wildtype colorectal cancer

Valérie M. Wouters[1,2], Roxan F. C. P. A. Helderman[1,2], Kate Cameron[1,2], Sander R. van der Hooff[1,2], Arezo Torang[1,2], Saskia van den Bergh[1,2], Rene Jackstadt[3], Owen J. Sansom[4,5], Sanne M. van Neerven[6] and Jan Paul Medema[1,2]✉

Colorectal cancer (CRC) can be divided into 4 subtypes of which consensus molecular subtype 4 (CMS4) is associated with metastasis and poor survival. Previously, we reported that the KPN mouse model resembles human CMS4. Strikingly, although tumor formation in this model is slow and limited, effective metastasis is observed. To understand this aggressive behavior, we compared two distinct in vitro KPN models, organoids and tumoroids. The organoid model only carries the original mutations, while the tumoroids are derived from in vivo grown tumors that underwent selection during development. Here, we reveal that tumoroids harbor endogenous WNT pathway activity, which can be driven by tankyrase activity and *Cdx2* downregulation. Importantly, WNT pathway activation was heterogeneous in nature, subject to regulation and allowed for a mixture of WNT-driven and YAP-driven cells within tumoroids. This unique type of WNT pathway activation is not crucial for colonic tumor growth, but results in metastatic spreading. Intriguingly, these findings reflect a specific subset of aggressive human CMS4 cancers that display low *CDX2* expression and lack of classical WNT pathway mutations, while having a higher tendency to metastasize. Together, these data propose a novel mechanism for WNT pathway activation that drives metastasis formation in aggressive CRC.

Oncogene (2025) 44:2091–2102; https://doi.org/10.1038/s41388-025-03365-5

INTRODUCTION

Colorectal cancer (CRC) is the second leading cause of cancer-related death worldwide [1]. Mortality rate is highest amongst patients diagnosed with metastasized CRC of which less than 20% survive after five years [2]. Importantly, treatment response remains suboptimal due to extensive inter- and intra-tumor heterogeneity. To characterize CRC features and improve therapy efficacy, many efforts have been made to stratify tumors based on their genetic expression profiles and resulted in the consensus molecular subtypes (CMS). This CMS classification comprises four unique subgroups, of which CMS1 is enriched for microsatellite instable (MSI) tumors and CMS2/3/4 contain mainly microsatellite stable (MSS) tumors [3]. Of the MSS tumors, CMS2 most closely resembles the 'canonical' phenotype that is characterized by WNT/MYC pathway activation, which is associated with the sequential accumulation of classical mutations in CRC driver genes (Vogelgram) [4]. CMS3 is considered the more metabolically adapted subtype, whilst CMS4 is characterized by high stromal influx and epithelial-to-mesenchymal transition (EMT) signatures [3]. Of these subtypes, CMS4 is the most aggressive type with the poorest prognosis, as these tumors are prone to metastasize [3, 5–8]. Critically, understanding the molecular mechanisms underlying this metastatic potential will greatly contribute to improved and targeted therapeutic interventions for patients with CRC. We have previously generated a specific CMS4 mouse model which harbors a $Kras^{G12D}$ mutation, *Trp53* deletion and *Notch1* intracellular domain (ICD) overexpression using Cre recombinase-driven *loxP* recombination, known as the KPN model [9]. We demonstrated that tumors arising in this model display CMS4-like gene expression and spontaneously metastasize to the liver, lungs, and peritoneal cavity, thereby recapitulating the aggressive form of human CRC [9]. Surprisingly, KPN tumors displayed elevated levels of WNT activity although no mutations in major WNT pathway genes, such as *Apc* or *Ctnnb1*, were observed [9]. This is particularly interesting since increased WNT activity has been associated with oncogenic properties such as increased migration and metastasis (reviewed in [10]). Interestingly, inhibition of WNT ligand secretion in vivo using a porcupine inhibitor had no major effects on tumor development and metastatic potential in the KPN model [9]. Together, these data suggest that KPN tumors do not rely on extrinsic WNT ligands. Given the prolonged latency period exceeding 100 days, observed in this model's tumor development,

[1]Laboratory of Experimental Oncology and Radiobiology, Cancer Center Amsterdam, Amsterdam UMC, University of Amsterdam, van der Boechorststraat 6b, 1081BT Amsterdam, The Netherlands. [2]Oncode Institute, Amsterdam, The Netherlands. [3]Heidelberg Institute for Stem Cell Technology and Experimental Medicine (HI-STEM GmbH), Heidelberg, Germany. Cancer Progression and Metastasis Group, German Cancer Research Center (DKFZ), Im Neuenheimer Feld 280, 69120 Heidelberg, Germany. [4]CRUK Scotland Institute, Garscube Estate, Switchback Road, Glasgow G61 1BD, UK. [5]School of Cancer Sciences, University of Glasgow, Garscube Estate, Switchback Road, Glasgow G61 1QH, UK. [6]Wellcome Trust–Cancer Research UK Gurdon Institute, University of Cambridge, CB2 1QN Cambridge, UK. Subject Ontology colorectal cancer (CRC), consensus molecular subtype (CMS), organoids, tumoroids WNT signaling pathway, metastasis. ✉email: j.p.medema@amsterdamumc.nl

Received: 27 September 2024 Revised: 14 February 2025 Accepted: 20 March 2025
Published online: 6 April 2025

it is plausible that additional genetic or epigenetic adaptations, beyond the original Cre-driven mutations, have accumulated over time due to in vivo selection. Understanding this adaptation, which contributes to the aggressive phenotype observed in the KPN model, may provide further insight into the ontogeny of CRC. In this study, the mechanisms underlying this selective pressure were investigated by comparing KPN-mutant cells induced in vitro and in vivo as organoid and tumoroid cultures, respectively. A strong upregulation of WNT pathway activity in KPN tumoroids was observed and inhibition of the pathway was only shown with inhibitors downstream of extracellular ligand-receptor interaction. Tankyrase (TNKS) and the transcription factor CDX2 were identified as regulators of this intracellular WNT pathway activation. Furthermore, WNT pathway activation was heterogeneous and KPN tumoroids represent a mixture of cells that express high WNT pathway activation or high Yap activation and WNT signaling was shown to be crucial for the induction of metastasis. Intriguingly, a subset of CMS4 patients with *CDX2* low and *APC/CTNNB1*-wildtype tumors represent a group of CRCs that have a relatively high propensity to metastasize. Together, these findings suggest that the KPN recapitulates a subset of aggressive human CRC and provides insight into the requirement for WNT pathway activity in metastatic spreading. In addition, they point to a crucial role for TNKS and CDX2 in mediating this intrinsic WNT signaling.

MATERIALS AND METHODS

Mice breeding and tumoroid/organoid isolation

A genetically engineered mouse model with the following genotype was used: *Kras*$^{LSL\text{-}G12D/+}$, *Trp53*$^{fl/fl}$, Rosa26$^{LSL\text{-}N1icd/+}$ (KPN, C57BL/6, $N = 5$, mixed background) to introduce recombination of the target genes flanked by *loxP* sites with use of the enterocyte-specific Villin-Cre^{ERtm} promoter. To generate organoids, the proximal part of the small intestine of a non-induced mouse was used and organoid isolation was performed as described previously [11]. Mutations were induced by in vitro recombination upon tamoxifen addition (see section on organoid/tumoroid culture). To generate tumoroids, mutations were induced by in vivo recombination via intraperitoneal administration of a single injection of 2 mg tamoxifen (T5648, Sigma-Aldrich, the Netherlands) at an age of 6–12 weeks. Mice were sacrificed at clinical endpoint (weight loss and/or hunching and/or cachexia). Tumoroids were derived from the primary tumor of the small intestine and processed as described before [9]. Animal breeding, for isolation of the tumor and the proximal part of the small intestine, was performed in accordance with the UK Home Office regulations (Project License 70/8646) and all protocol used to obtain normal or cancerous intestinal tissue were subject to review by the Animal Welfare and Ethical Review Board of the University of Glasgow.

Animal transplantations

Needle-guided intracolonic transplantation. One full well of a 6-well plate was used to harvest organoid cultures that were mechanically dissociated and resuspended in 70 µl PBS per injection per mouse (female Hsd:Athymic Nude-*Foxn1*^{nu}, $N = 8$ per group) for colonic submucosal injections as described before [12], using a Karl Storz TELE PACK + VET endoscopic video unit (Storz, Germany). Mice were weighed twice per week and colonic tumor growth was measured once every 2 weeks using endoscopy. Mice were sacrificed 18 weeks post injection or when humane endpoint was reached (80% of the colon was blocked by the tumor, weight loss >20% of maximum weight, abnormal behavior, colon perforation). Colon, liver, lungs, spleen, diaphragm and peritoneum were analyzed for metastasis.

Intraperitoneal tumor outgrowth. One hundred thousand single cells (derived from organoids or tumoroids) were resuspended in 100 µl Matrigel:PBS (1:1), consisting of 50% fresh cold Matrigel (Corning, the Netherlands) and 50% PBS, and injected intraperitoneally per mouse (female Hsd:Athymic Nude-*Foxn1*^{nu}, $N = 6$ per group) as described previously [13]. Mice were weighed twice per week. Mice were sacrificed eight weeks after injection or when the humane endpoint was reached (ascites formation, weight loss >20% of maximum weight, abnormal behavior). As described in ref. [14], the peritoneal cavity was divided into 9 regions and each region was scored according to tumor size and incidence to derive a peritoneal cancer index (PCI) score. No blinding was performed during examination of the peritoneum.

Female mice (Hsd:Athymic Nude-*Foxn1*^{nu}, 6–12 weeks old) were purchased from Envigo and housed in a 12 h light/12 h dark cycle, with temperatures between 20 °C and 24 °C and 40–70% humidity. Before transplantation into mice, in vitro cultured organoids/tumoroids were seeded for 72 h in culture medium (as described in section 'organoid/tumoroid culture') before harvesting in Cell Recovery Solution (354253, Corning) on ice for 30 min to dissolve the Matrigel. To obtain single cells, organoids/tumoroids were harvested in TrypLE (12604013, Thermo Fisher Scientific, the Netherlands) for 3 min at 37 °C.

Animals were randomly assigned to organoid or tumoroid transplantation group and no blinding was performed during examination.

Organoid/tumoroid culture

Tumoroids and organoids were cultured in Matrigel (Corning, the Netherlands) and culture medium, composed of basal medium (ADF) with freshly added mouse EGF (50 ng/ml, 315-09, Thermo Fisher Scientific), R-spondin (20% (v/v) of in-house produced conditioned medium) and Noggin (10% (v/v) of in-house produced conditioned medium). ADF medium consists of advanced DMEM F/12, N2 (100x diluted) and B27 (50x diluted) supplements, 10 mM HEPES, 100 units/ml of penicillin, 100 µg/ml of streptomycin, 0.25 µg/ml amphotericin B and 2 mM Glutamax (all Gibco, the Netherlands). To recombine target genes containing *loxP* sites in organoids in vitro, 1 µM 4-hydroxytamoxifen (4-OHT, H7904, Sigma-Aldrich) was added to the culture medium overnight and refreshed with plain culture medium the day after. Cultures were maintained in humidified air containing 5% CO_2 at 37 °C.

DNA isolation, PCR and genotyping

The NucleoSpin Tissue kit (740952, Bioké, the Netherlands) was used to extract DNA according to manufacturer's guidelines. Per PCR reaction, 100 ng DNA and genotype-specific forward and reverse primers were added to MyTaq HS Red mix (25048, Bioline, Germany). Used primer sequences are listed in Supplementary Table 1.

Constructs, transfection and lentiviral transduction

To generate a constitutive *Cdx2* overexpression construct, *Cdx2* cDNA was excised with XhoI (R0146S, NEB, MA, USA) from pLV-tetO-Cdx2 (70697, Addgene, MA, USA) and cloned between the XhoI restriction sites of the pCW-CMV-FLAG-puro plasmid (a kind gift from Dr. Wouter Karthaus, EPFL, Lausanne, Switserland). To create a CRISPR knockout (KO) for *Cdx2*, lentiCRISPRv2-mCherry plasmid (99154, Addgene) was used carrying single-guide RNA targeting exon 1 (Supplementary Table 2) via Bsmb1 cloning (R0580, NEB). A WNT reporter with iRFP713 expression (designated pMULE-TOP-iRFP713) was produced by simplifying the pMULE_CMV-eGFP_TOP-iRFP_PTCH1-mTurquoise2_CBF-tdTomato plasmid (113865, Addgene) via SalI restriction digestion of the PTCH1 and CBF reporter parts. Stbl3 competent bacteria (C737303, Thermo Fisher Scientific) were used for transformation, NucleoSpin Plasmid EasyPure (740727, Bioké) was used for plasmid isolation, and successful cloning was validated by Sanger sequencing with use of the BigDye Terminator (BDT) v1.1 sequencing kit (4337452, Thermo Fisher Scientific). Lentiviruses were produced by HEK293T cells using second-generation packaging plasmids VSV.G (14888, Addgene) and psPAX2 (12260, Addgene) and desired lentiviral construct in a ratio of 1:3:4 via Lipofectamine 2000 transfection reagent (11668019, Thermo Fisher Scientific). Organoids/tumoroids were transduced by spinoculation with culture medium, 10 µM ROCK inhibitor (Y0503, Sigma-Aldrich) and 8 µg/ml polybrene (107689, Sigma-Aldrich) containing lentiviral particles at 32 °C for 1 h and incubated overnight in humidified air containing 5% CO_2 at 37 °C before transferring them to Matrigel. Tumoroids, transduced with the pCW-*Cdx2* overexpression construct, were selected with puromycin (1 µg/ml, ant-pr-1, Invivogen, the Netherlands). *Cdx2* overexpression was validated via reverse transcription quantitative PCR (RT-qPCR). Organoids or tumoroids transduced with lentiCRISPRv2-*Cdx2 or* pMULE-TOP-iRFP713 were single-cell sorted with the BD FACSAria III cell sorter (BD Biosciences, the Netherlands) based on the positive expression of construct-dependent fluorescent selection markers. After expansion of the unique CDX2 KO single cell clones, newly generated lines were validated for CRISPR editing of *Cdx2* by Sanger sequencing and TIDE analysis [15]. Single-cell clones carrying the WNT reporter were assessed for WNT reporter presence upon stimulation with the

GSK3β-inhibitor/WNT-activator CHIR-99021 (CHIR, 10-1279, Tebubio, the Netherlands) by flow cytometry.

RNA isolation, cDNA synthesis and RT-qPCR

The NucleoSpin RNA kit (740955, Bioké) was used to extract RNA, which was then synthesized into cDNA using SuperScript III RT (18080093, Thermo Fisher Scientific) according to the manufacturer's protocol. RT-qPCR was performed using SYBR Green mix (Roche, the Netherlands) and Ct values were measured on the LightCycler 480 II machine (Roche). Gene expression was calculated after normalization to the housekeeping gene *Rpl37*. Used primer sequences are listed in Supplementary Table 3.

Bulk RNA sequencing and data processing/analysis

RNA was extracted 72 h after seeding as described above. RNA Integrity Number (RIN) values were evaluated with RNA ScreenTape analysis on the Agilent 2100 Bioanalyzer (Agilent Technologies, CA, USA). Library preparation was done with the KAPA RNA Hyperprep (Roche) and samples were sequenced on the Illumina HiSeq4000 platform with ~30×10^6 reads per sample. Initial quality assessment of the raw data was conducted using FastQC (v0.11.9) and MultiQC (v1.9) [16, 17]. Cutadapt was used (v1.18) for trimming and removal of poor-quality bases (Phred score <20) per sequence [18]. Sequence alignment against the Genome Reference Consortium mouse genome build 38 (GRCm38) and gene count determination were performed using STAR (v2.7.4a) [19]. Assessment of differentially expressed genes and generation of Volcano plots were done using the Genomics Analysis and Visualization Platform 'R2' [20]. Gene set enrichment analysis (GSEA [21]), was used to run the 'GSEApreranked' tool with online available gene sets on a generated pre-ranked list based on log2 fold change expression of our own data including all genes.

Single cell RNA sequencing and data processing/analysis

KPN tumoroids were collected 72 h after seeding and digested as single cells as described above. Cells were gated for live cells on $DAPI^{neg}$ (D9542, Sigma-Aldrich) expression and sorted on the BD FACSAria III cell sorter (BD Biosciences). Live cells were manually counted and 10.000 cells were processed using 10x Chromium Single Cell 3'Reagent Kits v3 (v3.1 Chemistry Dual Index) and sequenced on the Illumina NovaSeq6000 platform. Reads were aligned against the GRCm38 and counted using the 10x Genomics Cellranger software (v3.1.0). Seurat library in R was used to analyze raw count matrices. Assessment of gene expression was done using the Genomics Analysis and Visualization Platform 'R2' [20].

Flow cytometry

Organoids/tumoroids were harvested for single-cell processing as described above. Single cells were harvested in PBS and flow cytometry analysis or FACS were performed on the BD LSRFortessa (BD Biosciences) or BD FACSAria III cell sorter (BD Biosciences). Single cells were gated for live cells on $DAPI^{neg}$ (D9542, Sigma-Aldrich) expression. WNT reporter fluorescence expression (iRFP713) was measured with the 640 nm laser. LY6a (1:10.000, PE-conjugated, 12-5981-82, Thermo Fisher Scientific) and TROP2 (1:1000, AF1122, R&D systems, Minneapolis, MN, USA) + anti-Goat IgG (1:500, PE-conjugated, F0107, R&D systems) expression were measured with the 561 nm laser. Data was analyzed using FlowJo Software (BD).

Paraffin-embedding and immunohistochemistry/RNA-in situ hybridization (ISH)

Organoid/tumoroid cultures were washed with PBS and then fixed with 4% paraformaldehyde (PFA, 157-8, Electron Microscopy Sciences, the Netherlands) overnight at 4 °C and transferred to 70% ethanol the day after for 30 min at room temperature (RT), followed by dehydration with 100% ethanol containing hematoxylin (105175, Sigma-Aldrich; used for counterstaining) and repeated with 100% ethanol twice and xylene (28973, VWR, the Netherlands) twice for 30 min at RT. The samples were incubated twice in paraffin at 60 °C for 30 min, embedded in fresh paraffin, cooled to 4 °C, and stored at −20 °C till use.

Mouse-derived tumors/organs were fixed with 4% paraformaldehyde overnight at 4 °C, dehydrated with ethanol, and then transferred to butanol for 60 min at RT before embedding in paraffin overnight.

A microtome (Leica, Germany) was used to cut the paraffin-embedded blocks into 4 µm sections. Slides were deparaffinized and rehydrated with xylene and decreasing ethanol steps. For immunohistochemistry staining, antigen retrieval was performed with Epredia Lab Vision HIER buffer L (pH 6.0, TA135HBL, Thermo Fisher Scientific) or Tris-EDTA (pH 8.0, 10708976001, E9884, Merck, the Netherlands) combined with staining with anti-CDX2 (1:100, MU392A, BioGenex, the Netherlands) or anti-β-catenin (1:1000, 610153, BD Biosciences), respectively. Secondary antibodies used were anti-mouse-HRP (DPVB110HRP, Immunologic, the Netherlands) or anti-mouse-HRP (8021, EnVision FLEX, Agilent Dako, the Netherlands). For RNA-ISH (RNAscope), slides were stained according to manufacturer's protocol (ACD RNascope 2.5 HD-Brown) with probes against *Notum* (428981, ACD) or *Lgr5* (312171, ACD). Slides are visualized via DAB (BS04-999, Immunologic), counterstained with hematoxylin (105175, Sigma-Aldrich) and mounted using standard procedures according to manufacturer's protocols.

Western blotting

Organoids/tumoroids were collected in Cell Recovery Solution (354253, Corning) and placed on ice for 30 min to dissolve Matrigel and subsequently lysed using Laemmli sample buffer (1610737, Bio-Rad, the Netherlands) with Halt protease and phosphatase inhibitor cocktail (1:100, 78440, Thermo Fisher Scientific) and 1.4 M β-mercaptoethanol (M6250, Sigma-Aldrich). Protein concentrations were measured with Protein Quantification Assay kit (740967, Bioké) according to manufacturer's instructions and measured on a BioTek absorbance reader (Agilent). Protein samples (20 µg) were loaded into 4–15% precast gels (4561083, Bio-Rad) and transferred to polyvinylidene difluoride (PVDF) membranes using the Trans-Blot Turbo System (Bio-Rad). Membranes were blocked for 1 h in 5% bovine serum albumin (BSA, Sigma-Aldrich) in Tris-buffered saline plus 0.1% (v/v) Tween-20 (TBS-T, Sigma-Aldrich) followed by incubation with primary antibody overnight at 4 °C. The next day, membranes were washed with TBS-T, then incubated with secondary antibodies conjugated with horseradish peroxidase (HRP) for 1 h at RT and developed with Lumi-Light^{PLUS} Western Blotting Substrate (12015196001, Roche). Membranes were imaged on the ImageQuant LAS4000 (GE Healtcare Life Sciences, the Netherlands) and grayscale measurements were used to quantify protein levels, as previously described, and normalized to GAPDH levels [22]. Used antibodies were anti-β-catenin (1:1000, 9562, Cell Signaling Technology, the Netherlands), anti-GAPDH (1:5000, MAB374, Sigma-Aldrich), anti-vinculin (1:1000, 13901, Cell Signaling Technology), anti-rabbit-HRP (1:5000, 7074, Cell Signaling Technology) and anti-mouse-HRP (1:10.000, 1031-05, Southern Biotech, AL, USA).

Human datasets

Sweden set. A dataset of whole genome sequences and transcriptomes of 1063 primary CRCs from a recently published set ('Sweden set') was used for analysis of *CDX2* expression, CMS classification, *APC/CTNNB1* mutational status, MSS/MSI status and prognosis. The classification of CMS and MSS/MSI was assigned as reported in ref. [23]. Samples were categorized as mutant when at least 1 driver mutation in *APC* and/or *CTNNB1* was present. Mutations were called as drivers when the change was classified as 'oncogenic' or 'likely oncogenic' by the OncoKB web API (https://www.oncokb.org/). Expression was TPM-normalized and log2-transformed.

TCGA PanCancer Atlas set. TCGA PanCancer Atlas whole exome sequencing and RNA sequencing data for colon and rectal cancers were downloaded from cBioPortal for analysis of *CDX2* expression and *APC/CTNNB1* mutational status [24, 25]. *CDX2* mRNA levels were RSEM-normalized and log2-transformed [26]. Samples were categorized as mutant when at least 1 mutation in *APC* and/or in the region encoding the phosphorylation sites of CTNNB1 was present.

Sanger set. IC50 values of XAV-939 (TNKS inhibitor) of human colon and rectum adenocarcinoma sanger cell lines (COREAD) were available via Genomics of Drugs Sensitivity in Cancer (GDSC) database: (https://www.cancerrxgene.org/compound/XAV939/1268/overview/ic50?tissue=COREAD). Cell lines were categorized as mutant when at least 1 driver mutation in *APC* and/or *CTNNB1* was present. Mutations were called as drivers when the change was classified as 'oncogenic' or 'likely oncogenic' by the OncoKB web API (https://www.oncokb.org/). Assessment of *CDX2* gene expression was done using the Genomics Analysis and Visualization Platform 'R2' [20].

Statistical analysis

Statistics are performed using GraphPad Prism 10.2.0 for all figures, except for the analysis of patient tumor data where indicated. Here R version 4.3.2

was used. A p-value of <0.05 is considered significant. Sample size, *p*-values, error bar definitions and statistical testing are described in the figure legends.

Ethics approval

All methods were performed in accordance with the relevant guidelines and regulations. All animal transplantations were approved by the Animal Experimentation Committee at the Amsterdam UMC in Amsterdam (ethical approval numbers AVD11800202013801 and AVD11800202317163) and performed according to national guidelines. All used human data sets are published and publicly available.

RESULTS

WNT pathway activity in KPN models in vitro

The KPN model has been shown to grow aggressive tumors with high metastatic potential. However, tumor development is relatively slow and limited, as on average only two tumors per intestine develop with a latency of more than 100 days [9]. As a comparison, mouse models that harbor mutations in the most frequently mutated gene involved in CRC, *Apc*, combined with deletion of *Trp53*, will in the same setup develop at least 20 tumors [9]. This implies that additional changes are likely needed to promote tumor growth in the KPN model. Remarkably, KPN tumors appear to have elevated WNT activity, in the absence of mutations in *Apc* and in the majority of cases also without mutations in *Ctnnb1*. Nonetheless, these APC and β-catenin wildtype tumors do grow independently of exogenous WNT ligands. This suggests that, in the KPN model, alternative regulation of WNT signaling may play a role in stimulating tumor growth.

To investigate the nature of the in vivo adaptation that drives tumor growth within the KPN model, two different in vitro 3D cultures derived from the KPN mouse model were compared: KPN tumoroids and KPN organoids (Fig. 1a, b). The KPN tumoroids were derived directly from tumors that developed in vivo in the KPN mice, while KPN organoids were established from a healthy small intestine derived from an uninduced KPN mouse and were recombined in vitro by the addition of 4-OHT (validated in Supplementary Fig. 1a, b). As the latter have not been exposed to an in vivo selection pressure, these organoids are assumed to be without any additional mutations. To assess the difference between KPN tumoroids and organoids, mRNA was sequenced and differentially expressed genes (DEGs) were identified and analyzed for enrichment for known gene sets (Fig. 1c, d). Strikingly, tumoroids and organoids displayed significantly different expression profiles (Fig. 1c), and tumoroids were specifically enriched in genes involved in WNT signaling (Fig. 1d), confirming the in vivo adaptation in the KPN model, beyond the three initial mutations. To exclude genetic heterogeneity within the tumoroid cultures, single-cell clones derived from bulk tumoroids were grown and RNA was sequenced synchronously and compared to the KPN organoids for DEGs (Supplementary Fig. 2a–c). In agreement with the results observed in bulk cultures, gene set enrichment of upregulated genes in multiple single-cell KPN tumoroid clones confirmed the WNT signaling pathway as the top hit compared to KPN organoids (Supplementary Fig. 2a, b). Moreover, single-cell-cloned KPN tumoroids displayed elevated expression of known WNT pathway regulating genes and transcriptional targets, such as *Nkd1, Notum, Wif1*, *Axin2*, and *Lef1* (Supplementary Fig. 2c). These sequencing results were confirmed with RT-qPCR for WNT target gene *Axin2* levels in the single-cell clones (Supplementary Fig. 2d). To examine transcriptional regulation of the WNT pathway, cellular location of the β-catenin protein was analyzed with immunohistochemistry (IHC). This showed nuclear staining in the tumoroids but not in the organoids, suggesting increased transcription of β-catenin target genes in tumoroids (Fig. 1e, left panels). In agreement, *Notum* RNAscope confirmed the differences detected by mRNA sequencing (Fig. 1e, right panels). To directly measure WNT pathway activity, a fluorescent WNT signaling reporter was introduced into the organoids and tumoroids. This reporter measures nuclear activation of the transcription factors TCF/LEF upon β-catenin binding, quantified with a fluorescent marker. A strong reporter activation was observed in tumoroids, in sharp contrast to the organoids, which show very low WNT reporter activity (Fig. 1f, g).

WNT signaling is regulated independently of ligand-receptor interaction but depends on tankyrase activity and Cdx2 expression

To investigate WNT pathway activity in both models in more detail, the expression of the transcriptional WNT target *Axin2* was used as a read-out. Withdrawal of R-spondin1 or addition of the porcupine inhibitor LGK-974 was used to destabilize the WNT-receptor Frizzled (FZD) or inhibit WNT-ligand secretion from the cell, respectively (Fig. 2a). Compared to control samples (cultured in full ENR medium, consisting of EGF, Noggin and R-spondin1), KPN organoids were shown to rely on R-spondin1 and autocrine production of WNT ligands for *Axin2* transcription (Fig. 2b). In contrast, *Axin2* expression in tumoroids was not only much higher than in organoids (Supplementary Fig. 2d), but it was also expressed independently of exogenous WNT ligands (Fig. 2c). To identify possible factors involved in WNT signaling further downstream of the ligand-receptor interaction, the top 30 up- and downregulated genes between KPN tumoroids and organoids were analyzed in more detail. *Cdx2* was found as one of the top hits to be downregulated in these KPN tumoroids (Fig. 2d). Intriguingly, not all KPN tumoroids derived from tumors growing in KPN mice displayed *Cdx2* downregulation (Supplementary Fig. 3a**, case 6 and 7**). In some samples significant *Cdx2* expression was still observed, but this was invariable the case in KPN tumoroids that contained mutations in either *Ctnnb1* or displayed strong mutations in *Csnk1a1* (Supplementary Fig. 3b**, case 6 and 7**). In agreement, stronger WNT pathway activity was evident in these KPN tumoroid lines as compared to the KPN tumoroids with *Cdx2* downregulation, reaching levels of *Apc*-mutant organoids (Supplementary Fig. 3b). Together, these observations indicate that WNT pathway adaptation is crucial for tumor formation to occur in the KPN model and that the larger fraction of tumors developing do so by modulating *Cdx2* expression.

CDX2 has been reported to stimulate the transcription of *AXIN2* and *GSK3β*, which encode components of the cytoplasmic destruction complex that targets β-catenin for proteasomal degradation [27]. Therefore, decreased CDX2 expression could lead to increased WNT-pathway activity. mRNA levels of *Cdx2* were validated by RT-qPCR, which confirmed the very low expression levels in tumoroids compared to organoids (Supplementary Fig. 3c). To exclude that WNT signaling activity itself downregulated *Cdx2* expression, AKPN organoids (Villin-Cre^{ERtm}, *Apc*$^{-/-}$, *Kras*$^{G12D/+}$, *Trp53*$^{-/-}$, Rosa26$^{N1icd/+}$), which exhibit genetic activation of the WNT pathway due to *Apc* deletion, were checked for *Cdx2* expression; this showed even higher levels than KPN organoids, indicating that WNT pathway activation is not leading to *Cdx2* repression (Supplementary Fig. 3c). Differential CDX2 expression patterns were also detected at the protein level, using IHC, with no expression detected in KPN tumoroids, while KPN organoids showed nuclear CDX2 staining (Fig. 2e). To investigate the role of the β-catenin destruction complex in WNT activation in KPN tumoroids, an inhibitor that directly intervenes with the destruction complex was used. TNKS inhibition with IWR-1 leads to stabilization of AXIN and, subsequently, augments the activity of the destruction complex, diminishing Wnt pathway output (Fig. 2a). Interestingly, whilst KPN tumoroids were sensitive to IWR-1 and exhibited decreased WNT-target gene expression upon treatment (Fig. 2f, Supplementary Fig. 3d, e), KPN organoids were unresponsive to TNKS inhibition as they rely more on

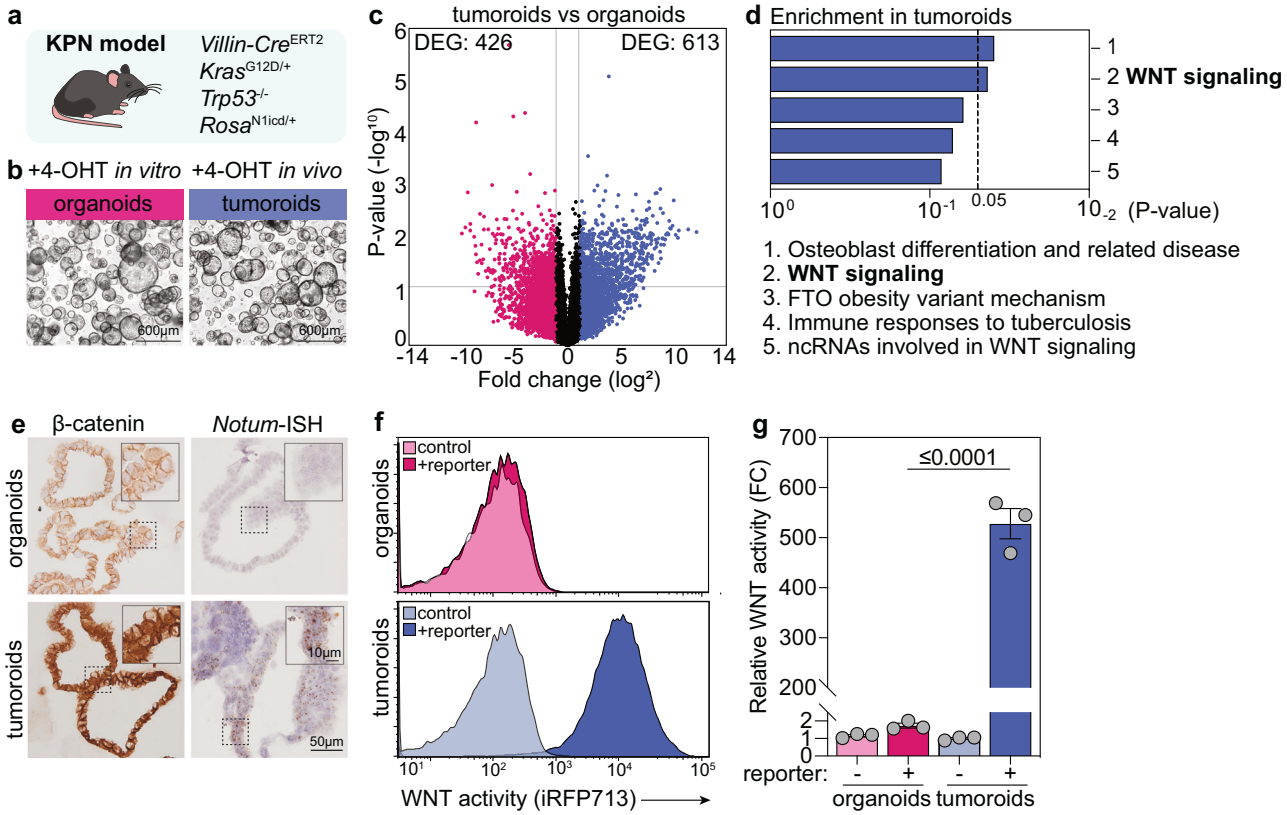

Fig. 1 In vitro cultured KPN organoids and tumoroids display differential WNT activity. a Schematic overview of the KPN mouse model. **b** Representative images of KPN organoids and tumoroids cultured 3D in Matrigel. Scale bar, 600 µm. **c** Volcano plot for differentially expressed genes (DEG) in tumoroids and organoids. Four tumoroid lines were derived from four different KPN mice ($N = 4$). Two organoid lines were derived from two different KPN mice and two independent experiments were performed ($N = 4$). Pink denotes downregulated genes in tumoroids with log2 fold change >-1, blue denotes upregulated genes in tumoroids with log2 fold change >1. **d** Wiki Pathways gene set enrichment (WP428) of 1000 most upregulated genes (fold change >1, $p < 0.05$) in tumoroids (bulk). **e** IHC staining for β-catenin protein or *Notum* in situ hybridization (ISH) on organoids and tumoroids. Scale bar, 50 µm. Scale bar zoom panel, 10 µm. **f** Flow Cytometry for WNT reporter activity measured on 640 nm laser. **g** Geometrical mean of WNT reporter fluorescence relative to untransduced parental cells lacking the WNT reporter. Dots represent $N = 3$ independent experiments. Data are mean±s.e.m and analyzed with unpaired two-tailed Student's *t* test.

ligand-receptor inhibition (Supplementary Fig. 3f). To demonstrate the selectivity of IWR-1 towards the destruction complex, AKPN organoids, which cannot assemble a functional destruction complex due to the absence of APC, were also treated and shown to be insensitive to IWR-1 (Supplementary Fig. 3g–i).

Cdx2 downregulation, as a consequence of CpG island methylation, in CRC has been extensively studied [28–30]. To determine whether *Cdx2* downregulation is mediated by gene methylation, KPN tumoroids were treated with decitabine, a DNA methyltransferase inhibitor. Upon hypomethylation, *Cdx2* expression was induced in KPN tumoroids (Supplementary Fig. 3j), pointing towards a similar mechanism as reported for CRC.

To gain more insight into the role of *Cdx2* downregulation in WNT signaling, KPN tumoroids were transduced with a lentiviral *Cdx2* overexpression construct (Supplementary Fig. 3k). *Cdx2* transcript levels were increased more than 700 times in comparison with untransduced KPN tumoroids, reaching levels comparable to those of the KPN organoids (Fig. 2g). Expression of downstream WNT targets was examined in tumoroids expressing either endogenous or overexpressed levels of *Cdx2* in the presence or absence of IWR-1. Both *Cdx2* overexpression and TNKS inhibition alone downregulated WNT target expression levels, but a combination of both these interventions had an even more significant impact (Fig. 2h, Supplementary Fig. 3l, m). Reciprocally, KPN organoids in which *Cdx2* was knocked out showed increased WNT pathway activity and expression of transcriptional target *Axin2* (Fig. 2i, j). *Cdx2* overexpression and TNKS inhibition, individually and combined, also decreased the protein levels of β-catenin in the tumoroids (Fig. 2k), in line with our hypothesis that both enhance the activity of the destruction complex leading to decreased transcriptional activity of the WNT pathway. Vice versa, increased protein levels of β-catenin were shown in KPN organoids with *Cdx2* KO and in combination with GSK3β-inhibitor CHIR-99021 (Fig. 2k), confirming that *Cdx2* is able to regulate the WNT pathway in the KPN model.

As reported by Jackstadt et al. [9], KPN tumors do not reach intrinsic WNT pathway signaling as high as APN tumors (Fig. 2l). Therefore, WNT pathway signaling in the KPN tumoroids was moderately active. Interestingly, APN tumors with hyperactivated WNT signaling do not metastasize, which is in line with recent discoveries highlighting the importance of the plasticity of two heterogenic cell states that drive metastasis [31–33]. These two heterogenic cell states maintain either high WNT activity or YAP activity and are defined by a crypt-base columnar stem cell (CBC)

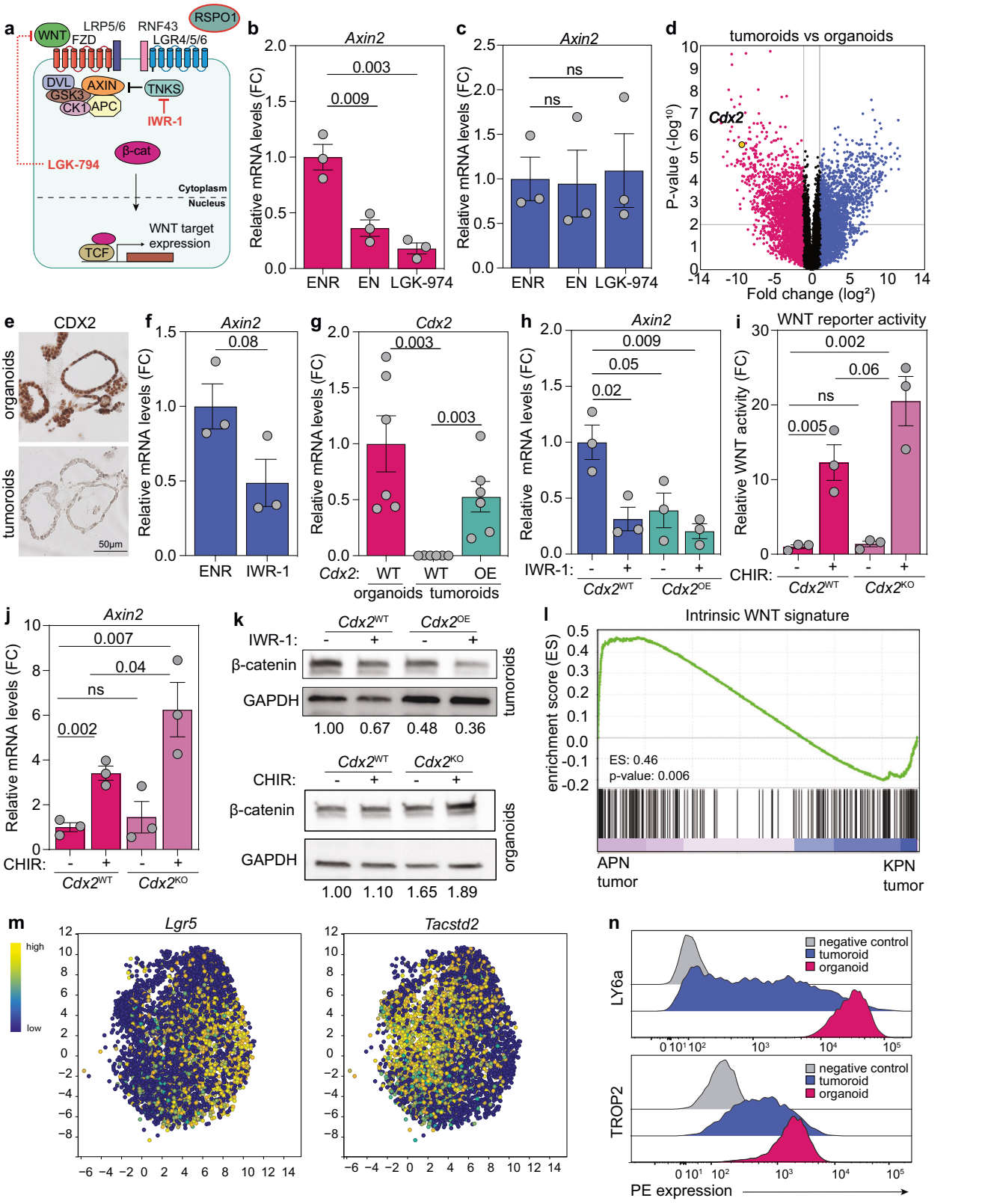

signature and regenerative stem cell (RSC) signature, respectively [33]. To determine whether KPN tumoroids also contained such heterogeneity, single cell sequencing was performed, which revealed two distinct cell populations. One has high levels of *Lgr5* (epithelial, WNT^{high} marker), while the other was more fetal/regenerative-like as defined by *Tacstd2* (YAP^{high} marker) (Fig. 2m). In addition, flow cytometry stainings for LY6a and TROP2, well-known YAP-driven markers of the fetal epithelium [34, 35], showed heterogenic expression in KPN tumoroids. In contrast, KPN organoids did not show heterogeneous staining and instead

Fig. 2 Tankyrase and the transcription factor CDX2 drive intrinsic WNT signaling in tumoroids. a Schematic overview of the WNT pathway and WNT pathway inhibitors used in this study. *Axin2* levels of KPN organoids (**b**) and tumoroids (**c**) cultured after 72 h of R-spondin withdrawal (EN) or LGK-974 (5 µM, S7143, Selleckhem, USA) treatment. Fold change (FC) relative to standard culture conditions (ENR). **d** Volcano plot highlighting expression of *Cdx2* among transcripts differentially expressed in KPN tumoroids vs KPN organoids. KPN tumoroids represent 3 independent experiments with 2 different tumoroid lines (single cell clones) derived from different mice ($N = 6$). KPN organoids represent 2 independent experiments with 2 different organoid lines (bulk) derived from different mice ($N = 4$). **e** Representative IHC staining for CDX2 in KPN organoids and tumoroids. **f** Levels of *Axin2* in KPN tumoroids after 72 h treatment with IWR-1 (10 µM, S7086, Selleckhem, USA). Fold change relative to standard culture conditions (ENR). Dots represent 3 independent experiments ($N = 3$). **g** Levels of *Cdx2* in KPN organoids and KPN tumoroids, and KPN tumoroids with *Cdx2* overexpression (OE). Fold change relative to expression levels in KPN organoids. Dots represent $N = 6$ independent experiments. **h** Levels of *Axin2* in untransduced KPN tumoroids and tumoroids with *Cdx2* OE after 72 h treatment with standard culture conditions (ENR) or IWR-1 (10 µM). Fold change relative to untransduced tumoroids cultured under standard culture conditions (ENR). Dots represent 3 independent experiments ($N = 3$). **i** Geometrical mean of WNT reporter fluorescence in KPN organoids after 48 h treatment with CHIR (5 µM) relative to untreated KPN parental cells lacking Cdx2 KO. Dots represent $N = 3$ independent experiments. Data analyzed with unpaired one-tailed Student's *t* test. **j** Levels of *Axin2* in untransduced KPN organoids and organoids with Cdx2 KO after 48 h treatment with standard culture conditions (ENR) or CHIR (5 µM). Fold change relative to untransduced organoids cultured under standard culture conditions (ENR). Dots represent 3 independent experiments ($N = 3$). Data analyzed with unpaired one-tailed Student's *t* test. **k** Representative western blot image for β-catenin protein levels in KPN tumoroids and tumoroids with *Cdx2* OE after 48 h treatment with IWR-1 (10 µM) or KPN organoids and organoids with Cdx2 KO after 48 h treatment with CHIR (5 µM). Values below image indicate the mean grayscale values of β-catenin relative to GAPDH levels from 3 independent experiments ($N = 3$). **l** GSEA of intrinsic WNT target genes (geneset derived from [61]) on pre-ranked (log2 fold change) mode for all differentially expressed genes in APN tumors ($N = 3$) compared to KPN tumors ($N = 7$) [9]. **m** Single cell RNA sequencing data for *Lgr5* and *Tacstd2* in KPN tumoroids ($N = 2$). **n** Flow Cytometry for LY6a or TROP2 expression (PE) measured on 561 nm laser. Data are mean ± s.e.m from $N = 3$ independent experiments, unless otherwise specified, and analyzed with unpaired two-tailed Student's *t* test.

had very high expression of these YAP^{high} markers (Fig. 2n). To determine the difference between KPN tumoroids and organoids in terms of dynamic cell states, gene set enrichment for CBC and RSC signatures was performed and confirmed the YAP^{high} state associated with the RSC signature in KPN organoids in comparison to tumoroids, while tumoroids were enriched for the WNT pathway activated CBC signature (Supplementary Fig. 4a,b). However, compared to APN tumors, KPN tumors are enriched for the RSC signature and were less purely WNT-driven (Supplementary Fig. 4c,d). Importantly, as the KPN tumoroids are clonally derived, the heterogeneity is installed dynamically. To conclude, KPN tumoroids maintain a dynamic heterogeneity for both WNT^{high} and YAP^{high} populations.

Elevated WNT signaling regulates metastatic potential in the KPN model

A crucial and unique aspect of the aggressiveness of the KPN model is the metastatic spreading to the lymph nodes, liver and lungs as well as to the peritoneal cavity, observed in nearly all tumor-bearing mice [9]. Given the high metastatic outgrowth in the KPN mouse model, the role of WNT activation on metastasis development was next examined. To study this, intracolonic transplantation of KPN tumoroids or KPN organoids was performed using endoscopic injection into the colon wall. Mice were killed either 18 weeks post transplantation or when endoscopic imaging showed 80% bowel obstruction by tumor growth (Fig. 3a, b and Supplementary Fig. 5a). Whereas all mice successfully transplanted with KPN tumoroids reached the end-point of 80% bowel obstruction, only 50% of the mice carrying KPN organoid transplants exhibited tumor outgrowth (Fig. 3c, d and Supplementary Fig. 5b), suggesting that the in vivo selection that KPN tumoroids had previously undergone increased their transplantation fitness. Nevertheless, the elevated WNT activity, achieved by the intracellular WNT pathway activation, was not crucial for tumors to grow after intracolonic injection as 50% of the KPN-organoid-transplanted mice did develop tumors (Fig. 3d). In contrast, 75% of the mice that showed KPN tumoroid outgrowth also developed metastasis, while none of the KPN-organoid-transplanted mice showed metastatic spreading (Fig. 3e and Supplementary Fig. 5c–e), not even when orthotopic tumor outgrowth was evident and had reached 80% bowel obstruction. To analyze the developed orthotopic tumors in more detail (Fig. 3f), lesions were checked for known marker expression. In accordance with the expression levels seen in 3D in vitro cultures and, in contrast to organoid transplants, tumoroid transplants showed increased levels of *Notum* and nuclear β-catenin and lacked CDX2 expression, as detected by RNAscope and IHC, implying that they retained their unique WNT pathway characteristics when transplanted in vivo (Fig. 3g). Interestingly, organoid transplants showed heterogeneous CDX2 protein expression (Fig. 3g) compared to uniform levels when cultured in vitro (Fig. 2e). In the transplanted mice, metastasis formation developed mostly in the liver and peritoneal cavity, recapitulating human disease and, specifically, the metastatic tropism of CMS4 CRCs (Fig. 3h,i) [7]. Importantly, heterogenic *Lgr5* expression in both colonic tumor and metastatic lesions of KPN tumoroid transplants was detected by in situ hybridization, and largely absent in KPN organoid derived transplants (Fig. 3j).

Although some mice injected with KPN organoids showed significant and relatively rapid tumor growth, the overall reduced number of tumors generated from transplanted KPN organoids could have affected their capacity to form metastases. Therefore, to directly assess the potential of growth of intestinal cells at distant sites, mice were injected intraperitoneally with KPN organoids or tumoroids and sacrificed 8 weeks after injection to examine outgrowth in the peritoneal cavity (Fig. 3k). Intriguingly, mice transplanted with KPN tumoroids had developed multiple tumor nodules, especially on the liver, omentum and back area of the peritoneal cavity, while mice injected with KPN organoids carried no or only a few small tumors (Fig. 3l, Supplementary Fig. 5f–h), again pointing to the requirement for WNT pathway activation and/or the heterogeneous WNT/YAP-active states for the outgrowth of metastases. Assessment of the PCI score further confirmed the significant difference in the metastatic growth of the two models (Fig. 3m, Supplementary Fig. 5i, j) [13]. In line with the orthotopic transplants, intraperitoneal organoid and tumoroid transplants also retained their expression patterns similar to those seen in vitro. KPN organoids-derived tumors maintained their WNT-low profiles, while the KPN tumoroid-derived tumors displayed WNT-activity in a subset of the cells (Fig. 3n).

The KPN tumoroid model closely resembles human CMS4 tumors in APC mutational status, CDX2 expression and prognosis

Based on transcriptomic analyzes, KPN tumoroids are classified as CMS4 and provide an aggressive mouse model for CRC recapitulating some of the metastatic features observed in patients [9]. Therefore, to determine whether KPN-tumoroid-specific characteristics, such as

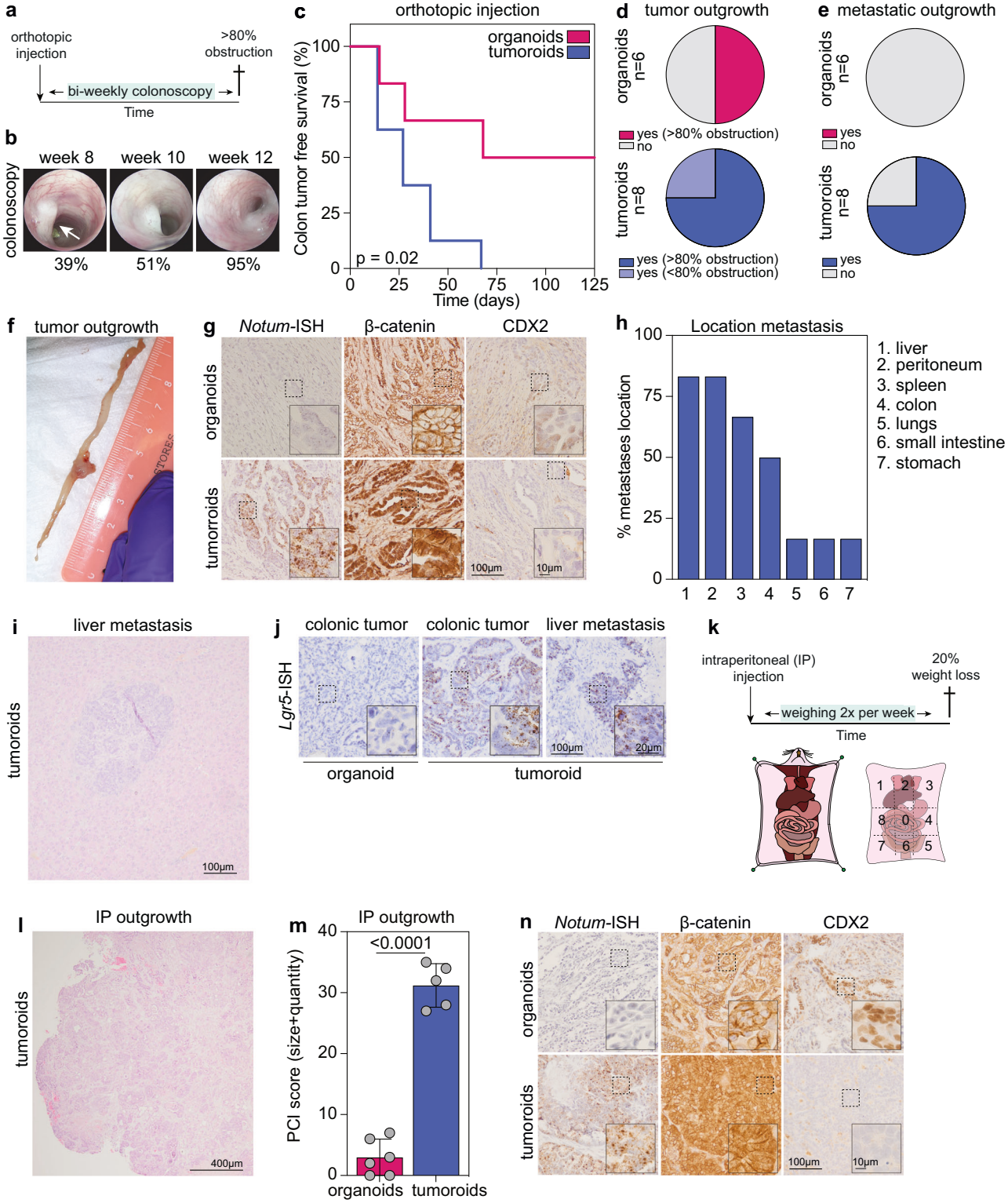

Apc/Ctnnb1 mutation-independent WNT pathway activation, low *Cdx2* expression and presence of metastases, were mirrored in human pathology, both the TCGA COREAD cohort (TCGA set) and a recently published human CRC cohort (Sweden set) were used [23, 36].

To exclude a confounding impact of microsatellite instability, which correlates with low *CDX2* expression [37–39], only MSS samples with variable levels of *CDX2* expression, including a subset showing low or no expression, were analyzed from the Sweden set (Fig. 4a). Although the MSS/MSI status was unknown for most patients, the variable *CDX2* expression was reproduced in the TCGA set when all patients were included (Supplementary Fig. 6a). To determine whether *CDX2* expression is correlated with classical WNT pathway mutations, the Sweden patient set was further separated into two groups based on the presence or absence of mutations in the *APC* or *CTNNB1* genes, the main driver mutations responsible for WNT hyperactivation in CRC. Strikingly,

Fig. 3 Metastatic potential of organoids vs tumoroids in vivo. a Schematic overview of in vivo experiment with intracolonic injection of KPN tumoroids and organoids. **b** Representative endoscopic images of colonic tumor growth over time till endpoint was reached (> 80% bowel obstruction). Arrow indicates tumor. **c** Kaplan-Meier curve of colon tumor-free survival. Organoids, $n = 6$; tumoroids, $n = 8$. Data analyzed by log-rank test. **d** Proportion of tumor growth in colon analyzed at human/clinical endpoint. **e** Proportion of presence of metastasis at human/clinical endpoint. **f** Representative image of intestine with tumor at clinical endpoint (> 80% bowel obstruction). **g** Representative *Notum* ISH and β-catenin/CDX2 IHC staining on colonic tumors derived from organoid and tumoroids. Insets represent zoomed-in images of dashed areas. Scale bar, 100 μm. Scale bar zoom panel, 10 μm. **h** Location of metastases originating from tumor grown from intracolonic tumoroid transplantation. **i** H&E staining of liver with metastasis derived from intracolonic tumoroid transplantation. Scale bar, 100 μm. **j** Representative *Lgr5* ISH on tumors derived from intracolonic tumoroid / organoid transplantation and liver metastasis derived from intracolonic tumoroid transplantation. Insets represent zoomed-in images of dashed areas. Scale bar, 100 μm. Scale bar zoom panel, 20 μm. **k** Schematic overview of in vivo experiment with intraperitoneal (IP) injection and PCI-scoring areas. **l** H&E staining of IP tumor grown from IP tumoroid transplantation. Scale bar, 400 μm. **m** PCI score including tumor size and quantity. Organoids $N = 6$, tumoroids $N = 5$. Data mean ± s.e.m;, analyzed with unpaired two-tailed Student's *t* test. **n** *Notum* ISH and β-catenin/CDX2 IHC staining on IP tumors derived from IP transplantations of organoids or tumoroids. Insets represent zoomed-in images of dashed areas. Scale bar, 100 μm. Scale bar zoom panel, 10 μm.

we found that around 20% of the MSS patients do not carry such a classical mutation and, importantly, this genetic subgroup associated strongly with significantly lower *CDX2* expression (Fig. 4b). In line with this observation, the patient population with the 25% lowest *CDX2* expression included fourfold more *APC/CTNNB1*-wildtype patients, compared to the group that contained the 25% highest *CDX2* expressing patients (Fig. 4c). These findings were replicated in the TCGA COREAD dataset (Supplementary Fig. 6b,c). This suggests that the combination of *Apc/Ctnnb1*-wildtype status and low *Cdx2* expression, observed in the KPN tumoroid model, is recapitulated in human CRC disease, potentially pointing to a similar mechanism of activating the WNT pathway. Furthermore, the value of the tankyrase inhibition on *CDX2*low/*APC/CTNNB1*-wildtype was analyzed using the GDSC database and revealed lower IC50 values for a known tankyrase inhibitor (XAV-939) for this subset compared to *CDX2*high/*APC/CTNNB1*-wildtype or *CDX2*high/*APC/CTNNB1*-mutant lines (Supplementary Fig. 6d). Together, these observations support our hypothesis that *CDX2* reduction and tankyrase activation typify this subset of CRCs.

Importantly, *APC/CTNNB1*-wildtype patients were more overrepresented in CMS4 patients compared to all other subtypes (Fig. 4d). Similarly, CMS4 patients were significantly enriched in the 25% lowest *CDX2*-expressing patient subgroup (55.9%) compared to the 25% highest CDX2-expressors (19.7%) (Fig. 4e). To investigate the clinical relevance of our findings, CMS4 was separated into *CDX2*high/*APC/CTNNB1*-mutant and *CDX2*low/*APC/CTNNB1*-wildtype and compared to a recently defined new classification system, intrinsic-consensus molecular subtypes (iCMS), that used intrinsic epithelial signatures to identify two subgroups, iCMS2 and iCMS3 [40]. These two subgroups are associated with different outcomes in CMS4 patients, of which iCMS3/CMS4 tumors have the worst prognosis [40]. Intriguingly, *CDX2*high/*APC/CTNNB1*-mutant CMS4 patients were mostly classified as iCMS2, while *CDX2*low/*APC/CTNNB1*-wildtype CMS4 patients were classified as iCMS3 (Fig. 4f). Since iCMS3 is associated with worse prognosis, the overall survival of these subgroups was determined. This showed significant differences, with *CDX2*low/*APC/CTNNB1*-wildtype CMS4 patients found to have worse outcome, in agreement with their corresponding iCMS classification (Fig. 4g). In addition, the association with the presence of metastasis was studied in CMS4 patients. In line with earlier findings [28, 41, 42], *CDX2*low/*APC/CTNNB1*-wildtype CMS4 patients were associated with a higher incidence of metastasis (Fig. 4h). Based on these results, we conclude that low *CDX2* expression is associated with *APC/CTNNB1*-wildtype patients and both features are enriched in CMS4 patients, more specifically in a subgroup of CMS4 patients that present with a high propensity to metastasize.

DISCUSSION

The role of canonical WNT hyperactivation in an *APC*-mutated setting has been reported extensively in CRC, since APC is generally considered as the main initiating event in the MSS canonical WNT-driven CRCs. As *APC* and *CTNNB1* are mutated in approximately 75% of all CRC cases [24], such patients possess a dysfunctional destruction complex and are therefore unable or ineffective at targeting β-catenin for degradation, resulting in the accumulation of this protein so that it can freely translocate to the nucleus and activate the WNT transcriptional program. Importantly, such *APC*-mutated CRCs do not present as null mutants and some residual control on β-catenin expression levels is evident [43]. This canonical WNT pathway hyperactivation is typically seen in CMS2 tumors, defined by high levels of classical WNT pathway targets and indeed holds the highest percentage of *APC* mutations. In contrast, CMS4 tumors contain relatively more *APC* wildtype tumors compared to the other MSS subtypes (CMS2 and CMS3). However, the majority of these CMS4 patients still show relatively high WNT pathway activity [3]. Currently, the KPN model is the best genetically modified mouse model for CMS4, which also lacks genetic perturbation of the *Apc* and *Ctnnb1* genes in contrast to most mouse models of CRC. Our study now shows that a unique mode of WNT pathway activation is the result of TNKS activity and *Cdx2* repression. TNKS inhibitors have been developed to target WNT pathway activity and applied to various models of CRC to test sensitivity [44–47]. Interestingly, results indicated that the effectiveness of TNKS inhibitors depended on the extent of the *APC* truncation with weaker mutations not responding [47]. Our two KPN models also showed variable sensitivity to TNKS inhibition. Moreover, human MSS CRC cell lines with wildtype APC and CTNNB1 and low CDX2 appear more sensitive to TNKS inhibition.

Our data also suggest that WNT activity in CMS4 patients, lacking *APC* mutations, could be partly regulated by *CDX2* downregulation, similarly to the CMS4 KPN tumoroid model. Importantly, recent data suggest that dynamic cell states are crucial for metastasis to occur in CRC. Fumagalli and co-workers indicated in mouse models that LGR5- cells travel through the circulation and seed at distant sites where they subsequently need to acquire WNT pathway activity and a subset of LGR5+ cells appear [31]. Similarly, Heinz et al. indicated that these two cellular states are defined by YAP and WNT activity respectively and are dynamically changing their expression profiles [32]. Intriguingly, this heterogeneity is mirrored in gene expression data of human CRCs with poor prognosis where a mixture of YAP-driven fetal gene expression (RSC) signatures with WNT-driven crypt-based columnar stem cell (CBC) signatures are associated with poor outcome for patients [33]. We observed that KPN tumoroids share this heterogeneity in cell states, while in contrast expression profiles of KPN organoids are purely YAP^{high} and APC-mutant driven organoids and tumoroids are largely WNT^{high}. The presence of this heterogeneity aligns with the potential to metastasize in mouse models, which is evident for KPN tumoroids but not for organoids and also not observed in the APC-driven models. We therefore believe that this heterogeneity underpins the metastatic potential of cancer cells in this mouse model and extends towards

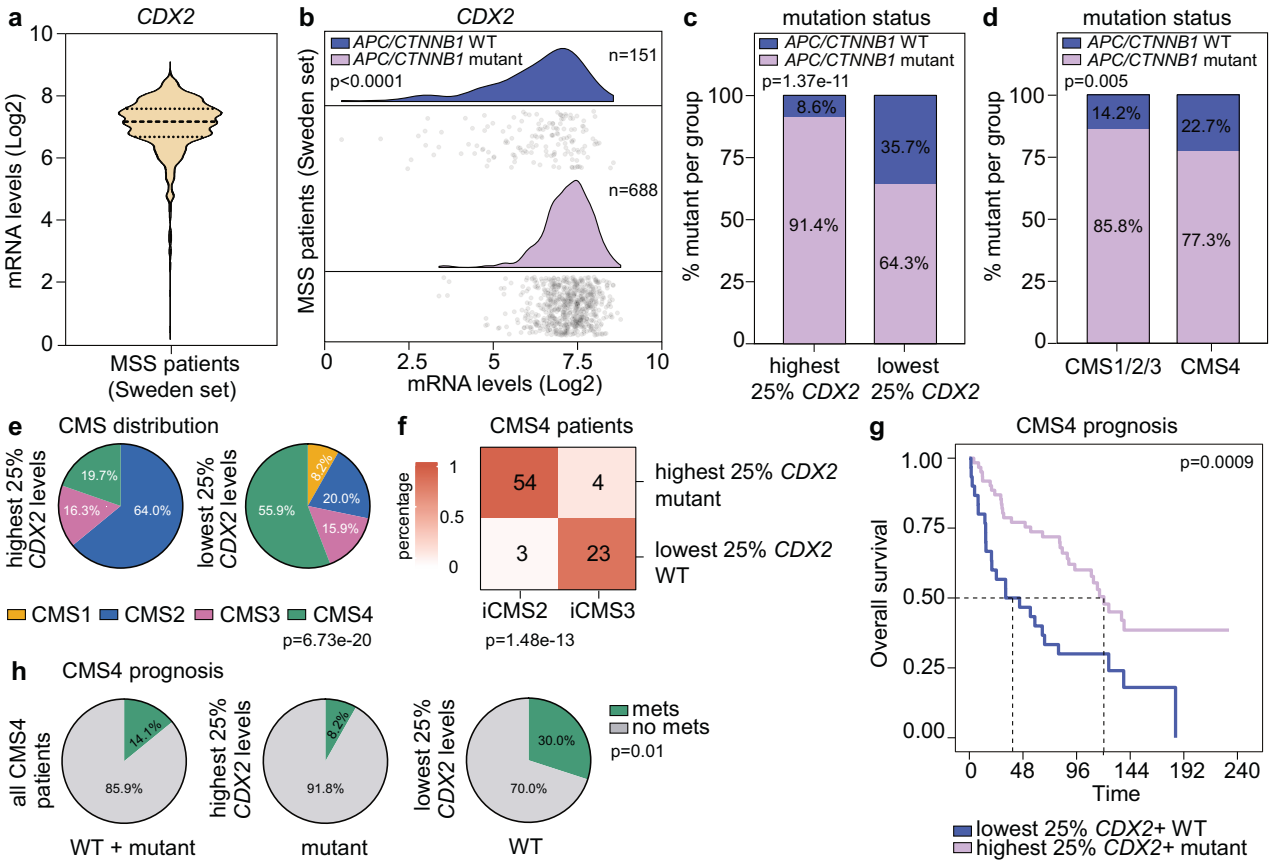

Fig. 4 Correlation of human *CDX2* expression with *APC/CTNNB1* mutation, CMS and metastasis in Sweden set. a *CDX2* levels in MSS patients, $n = 839$. Violin plot displays median and quartiles. **b** Comparison of *CDX2* expression in 2 groups based on *APC* and *CTNNB1* mutational status. WT = wildtype, $n = 151$. mutant, $n = 688$. Dots represent individual patients. Data analyzed with unpaired two-tailed Student's *t* test. **c** Comparison of *APC/CTNNB1* mutational status in 2 groups based on *CDX2* expression levels (25% highest vs 25% lowest expressors). $N = 210$ for both groups. Percentages are normalized within each group. Data analyzed with Fisher's exact test. **d** Comparison of *APC/CTNNB1* mutational status in 2 groups based on CMS classification. CMS1/23; $n = 431$, CMS4; $n = 255$. Percentages are normalized within each group. Data analyzed with Fisher's exact test. **e** CMS distribution within 25% of patients with highest *CDX2* levels versus CMS distribution within 25% of patients with lowest *CDX2* levels. $N = 210$ for both groups. Data analyzed with Fisher's exact test. **f** Confusion matrix calculated for iCMS2 or iCMS3 score within CMS4 patients. Groups are based on 25% highest *CDX2* expressors within CMS4 patients, mutant for *APC/CTNNB1* ($n = 61$, 58 iCMS classified and 3 patients undefined for iCMS classification) or on 25% lowest *CDX2* expressors within CMS4 patients, WT for *APC/CTNNB1* ($n = 30$, 26 iCMS classified and 4 patients undefined for iCMS classification). Data analyzed with Fisher's exact test. **g** Kaplan-Meier curve for overall survival calculated for groups based on 25% highest *CDX2* expressors within CMS4 patients, mutant for *APC/CTNNB1* ($n = 61$) or on 25% lowest *CDX2* expressors within CMS4 patients, WT for *APC/CTNNB1* ($n = 30$). Data analyzed by Logrank test. **h** Pie charts comparing the percentage incidence of metastasis in all CMS4 patients (left) versus subsets of CMS4 patients; *APC/CTNNB1* mutant samples within 25% highest *CDX2* expressors (middle) versus *APC/CTNNB1* WT samples within 25% lowest *CDX2 (*right*)*. Percentages are normalized within each group. CMS4 patients, $n = 255$; *APC/CTNNB1* mutant 25% highest *CDX2* expressors CMS4, $n = 61$; *APC/CTNNB1* WT 25% lowest CDX2 *expressors* CMS4, $n = 30$. Difference between 25% highest and lowest expressors analyzed with Fisher's exact test. R version 4.3.2 was used for statistical analyses.

APC and β-catenin wildtype CRC. The potential to modulate WNT pathway activity, which is more evident in these wildtype cases, is crucial to switch states and therefore allows for more effective metastasis.

Although CDX2 is regarded as a transcription factor that drives cell type specification in the intestine [48, 49], regulation of β-catenin activity by CDX2 has been reported before and appears to dependent on a direct interaction with β-catenin [50]. Alternatively, CDX2 has been shown to mediate expression of *GSK3β* and *AXIN*, and loss of CDX2 can thus be expected to decrease the levels of these two proteins that are vital parts of the destruction complex [27]. Although the exact mechanism by which *Cdx2* expression is downregulated in the tumoroids is unclear, this decrease has been recognized to occur in CRC due to hypermethylation and has been previously shown to be associated with CMS4 [51, 52], which was confirmed in the current analysis. In addition, low levels of CDX2 have been extensively correlated to poor prognosis in CRC [53–55]. Similarly, the iCMS classification has resulted in the refinement of CMS and identified CMS4 patients with worse prognosis as iCMS3. In line with this, *CDX2*low/*APC/CTNNB1*-wildtype CMS4 patients were classified as iCMS3 and had poor poorer prognosis compared to *CDX2*high/*APC/CTNNB1*-mutant CMS4 patients. As described by Nunes et al., *APC*-wildtype is associated with poor prognosis [23]. However, our analysis provides a start of an explanation why this association is a poor predictor as shown by a population of lower *CDX2* expressors in *APC*-wildtype patients, which emphasizes the relevance of this combination. Accordingly, screening for CDX2 expression levels could aid in the prediction of (worse) outcome in patients, specifically in the *APC/CTNNB1*-wildtype subset.

Next to a clear prognostic association, our data also reveal a maybe unexpected requirement for WNT activation in metastatic spreading within this subgroup. That WNT activation is needed for initiation of tumor formation in the colon is a well-accepted fact

[56–58]. Surprisingly, the KPN model suggested that this is not an absolute requirement as KPN organoids without WNT pathway activation grew out effectively in 50% of the cases. Whether this is due to in vivo production of WNT ligands by the microenvironment or to the intrinsic properties of the tumor cells themselves has not been studied, but it is clear that the conditions that allow for colonic tumor growth of KPN organoids are not sufficient for metastatic spreading. This indicates that the intrinsic WNT pathway activation, observed in the KPN tumoroids, not only allows for more effective tumor growth but is crucial for driving metastatic growth. The in vivo selection that is uncovered here for the KPN model is therefore an essential adaptation for the aggressive metastatic behavior of these tumor cells and further implies that the three primary mutations alone are insufficient to fully recapitulate this outcome. WNT pathway activity was shown to be crucial for the migratory capacity of CRC cells, which is an essential first step in metastasis (reviewed in [59]). Moreover, recent data indicate that effective metastatic growth in CRC requires a transition into a YAP-activated fetal state during migration, but a subsequent reversion towards a WNT-active epithelial state when seeded at a distant site [31, 32, 60]. This transitory phase appears to align with poor prognosis in patients as well and may point to a crucial WNT-dependency in the outgrowth of metastases [33]. This would explain why KPN organoids, which contain the rare combination of those three founder mutations, do not spontaneously metastasize by themselves, and thus do not represent a reliable CMS4 model. The additional (epi-)genetic changes that occur in the KPN tumoroids provide us with a unique and tractable model system that resembles a clinically relevant CRC subgroup that can be identified based on the characteristics investigated in this study. The use of TNKS inhibitors, as well as other therapeutic strategies defined in the KPN model, could very well lead to a more effective therapy for these high-risk patients in the future.

DATA AVAILABILITY

The sequence libraries generated in this study are publicly available through the National Center for Biotechnology Information (NCBI) Gene Expression Omnibus (GEO) under accession GSE277663.

REFERENCES

1. Sung H, Ferlay J, Siegel RL, Laversanne M, Soerjomataram I, Jemal A, et al. Global Cancer Statistics 2020: GLOBOCAN Estimates of Incidence and Mortality Worldwide for 36 Cancers in 185 Countries. CA: A Cancer J Clin. 2021;71:209–49.
2. National Cancer Institute Surveillance E, and End Results Program. Cancer stat facts: colorectal cancer. https://seer.cancer.gov/statfacts/html/colorect.htmlAccessed.
3. Guinney J, Dienstmann R, Wang X, de Reyniès A, Schlicker A, Soneson C, et al. The consensus molecular subtypes of colorectal cancer. Nat Med. 2015;21:1350–6.
4. Fearon ER, Vogelstein B. A genetic model for colorectal tumorigenesis. Cell. 1990;61:759–67.
5. Feliu J, Gámez-Pozo A, Martínez-Pérez D, Pérez-Wert P, Matamala-Luengo D, Viñal D, et al. Functional proteomics of colon cancer consensus molecular subtypes. Br J Cancer. 2024;130:1670–8.
6. Ten Hoorn S, de Back TR, Sommeijer DW, Vermeulen L. Clinical value of consensus molecular subtypes in colorectal cancer: a systematic review and meta-analysis. J Natl Cancer Inst. 2022;114:503–16.
7. Lenos KJ, Bach S, Ferreira Moreno L, Ten Hoorn S, Sluiter NR, Bootsma S, et al. Molecular characterization of colorectal cancer related peritoneal metastatic disease. Nat Commun. 2022;13:4443.
8. Luo Q, Quan Y, Liu W, Wu Z, Qiu W, Liang W, et al. Seed and soil: consensus molecular subgroups (CMS) and tumor microenvironment features between primary lesions and metastases of different organ sites in colorectal cancer. Cancer Manag Res. 2024;16:225–43.
9. Jackstadt R, van Hooff SR, Leach JD, Cortes-Lavaud X, Lohuis JO, Ridgway RA, et al. Epithelial NOTCH signaling rewires the tumor microenvironment of colorectal cancer to drive poor-prognosis subtypes and metastasis. Cancer cell. 2019;36:319–36.e7.
10. He K, Gan WJ. Wnt/β-catenin signaling pathway in the development and progression of colorectal cancer. Cancer Manag Res. 2023;15:435–48.
11. Ramesh P, Kirov AB, Huels DJ, Medema JPIsolation. Propagation, and clonogenicity of intestinal stem cells. Methods Mol Biol. 2019;2002:61–73.
12. Roper J, Tammela T, Cetinbas NM, Akkad A, Roghanian A, Rickelt S, et al. In vivo genome editing and organoid transplantation models of colorectal cancer and metastasis. Nat Biotechnol. 2017;35:569–76.
13. Bastiaenen VP, Klaver CEL, van der Heijden MCS, Nijman LE, Lecca MC, Tanis PJ, et al. A mouse model for peritoneal metastases of colorectal origin recapitulates patient heterogeneity. Lab Invest. 2020;100:1465–74.
14. Helderman RFCP, Restrepo MT, Rodermond HM, Bochove GGWV, Löke DR, Franken NAP, et al. Non-invasive imaging and scoring of peritoneal metastases in small preclinical animal models using ultrasound: a preliminary trial. Biomedicines. 2022;10:1610.
15. Brinkman EK, Chen T, Amendola M, van Steensel B. Easy quantitative assessment of genome editing by sequence trace decomposition. Nucleic Acids Res. 2014;42:e168.
16. Ewels P, Magnusson M, Lundin S, Käller M. MultiQC: summarize analysis results for multiple tools and samples in a single report. Bioinformatics. 2016;32:3047–8.
17. S. A. FastQC: a quality control tool for high throughput sequence data. http://www.bioinformatics.babraham.ac.uk/projects/fastqc 2010.
18. Martin M. Cutadapt removes adapter sequences from high-throughput sequencing reads. EMBnet J. 2011;17:10.
19. Dobin A, Davis CA, Schlesinger F, Drenkow J, Zaleski C, Jha S, et al. STAR: ultrafast universal RNA-seq aligner. Bioinformatics. 2013;29:15–21.
20. AUMC. R2 data base: Genomic Analysis And Visualization Platform, AUMC. http://r2.amc.nl 2023.
21. Subramanian A, Tamayo P, Mootha VK, Mukherjee S, Ebert BL, Gillette MA, et al. Gene set enrichment analysis: a knowledge-based approach for interpreting genome-wide expression profiles. Proc Natl Acad Sci USA. 2005;102:15545–50.
22. Buikhuisen JY, Gomez Barila PM, Torang A, Dekker D, de Jong JH, Cameron K, et al. AKT3 expression in mesenchymal colorectal cancer cells drives growth and is associated with epithelial-mesenchymal transition. Cancers. 2021;13:801.
23. Nunes L, Li F, Wu M, Luo T, Hammarström K, Torell E, et al. Prognostic genome and transcriptome signatures in colorectal cancers. Nature 2024;633:137–46.
24. Cerami E, Gao J, Dogrusoz U, Gross BE, Sumer SO, Aksoy BA, et al. The cBio cancer genomics portal: an open platform for exploring multidimensional cancer genomics data. Cancer Discov. 2012;2:401–4.
25. Gao J, Aksoy BA, Dogrusoz U, Dresdner G, Gross B, Sumer SO, et al. Integrative analysis of complex cancer genomics and clinical profiles using the cBioPortal. Sci Signal. 2013;6:pl1.
26. Li B, Dewey CN. RSEM: accurate transcript quantification from RNA-Seq data with or without a reference genome. BMC Bioinforma. 2011;12:323.
27. Yu J, Liu D, Sun X, Yang K, Yao J, Cheng C, et al. CDX2 inhibits the proliferation and tumor formation of colon cancer cells by suppressing Wnt/β-catenin signaling via transactivation of GSK-3β and Axin2 expression. Cell Death Dis. 2019;10:26.
28. Graule J, Uth K, Fischer E, Centeno I, Galván JA, Eichmann M, et al. CDX2 in colorectal cancer is an independent prognostic factor and regulated by promoter methylation and histone deacetylation in tumors of the serrated pathway. Clin Epigenetics. 2018;10:120.
29. Kim JH, Rhee YY, Bae JM, Cho NY, Kang GH. Loss of CDX2/CK20 expression is associated with poorly differentiated carcinoma, the CpG island methylator phenotype, and adverse prognosis in microsatellite-unstable colorectal cancer. Am J Surg Pathol. 2013;37:1532–41.
30. Dawson H, Galván JA, Helbling M, Muller DE, Karamitopoulou E, Koelzer VH, et al. Possible role of Cdx2 in the serrated pathway of colorectal cancer characterized by BRAF mutation, high-level CpG Island methylator phenotype and mismatch repair-deficiency. Int J Cancer. 2014;134:2342–51.
31. Fumagalli A, Oost KC, Kester L, Morgner J, Bornes L, Bruens L, et al. Plasticity of Lgr5-negative cancer cells drives metastasis in colorectal cancer. Cell Stem Cell. 2020;26:569–78.e7.
32. Heinz MC, Peters NA, Oost KC, Lindeboom RGH, van Voorthuijsen L, Fumagalli A, et al. Liver colonization by colorectal cancer metastases requires YAP-controlled plasticity at the micrometastatic stage. Cancer Res. 2022;82:1953–68.
33. Vasquez EG, Nasreddin N, Valbuena GN, Mulholland EJ, Belnoue-Davis HL, Eggington HR, et al. Dynamic and adaptive cancer stem cell population admixture in colorectal neoplasia. Cell Stem Cell. 2022;29:1213–28.e8.
34. Yui S, Azzolin L, Maimets M, Pedersen MT, Fordham RP, Hansen SL, et al. YAP/TAZ-dependent reprogramming of colonic epithelium links ECM remodeling to tissue regeneration. Cell Stem Cell. 2018;22:35–49.e7.
35. Mustata RC, Vasile G, Fernandez-Vallone V, Strollo S, Lefort A, Libert F, et al. Identification of Lgr5-independent spheroid-generating progenitors of the mouse fetal intestinal epithelium. Cell Rep. 2013;5:421–32.
36. Kirk S. The Cancer Genome Atlas Colon Adenocarcinoma Collection (TCGA-COAD) (Version 3) [Data set]. In: Lee Y, Sadow, C. A., Levine, S., Roche, C., Bonaccio, E., &

Filiippini, J., editor. The Cancer Imaging Archive. https://doi.org/10.7937/K9/TCIA.2016.HJJHBOXZ2016.
37. Slik K, Turkki R, Carpén O, Kurki S, Korkeila E, Sundström J, et al. CDX2 loss with microsatellite stable phenotype predicts poor clinical outcome in stage II colorectal carcinoma. Am J Surg Pathol. 2019;43:1473–82.
38. Baba Y, Nosho K, Shima K, Freed E, Irahara N, Philips J, et al. Relationship of CDX2 loss with molecular features and prognosis in colorectal cancer. Clin Cancer Res. 2009;15:4665–73.
39. Lugli A, Tzankov A, Zlobec I, Terracciano LM. Differential diagnostic and functional role of the multi-marker phenotype CDX2/CK20/CK7 in colorectal cancer stratified by mismatch repair status. Mod Pathol. 2008;21:1403–12.
40. Joanito I, Wirapati P, Zhao N, Nawaz Z, Yeo G, Lee F, et al. Single-cell and bulk transcriptome sequencing identifies two epithelial tumor cell states and refines the consensus molecular classification of colorectal cancer. Nat Genet. 2022;54:963–75.
41. Wang YS, Kou Y, Zhu RT, Han BW, Li CH, Wang HJ, et al. CDX2 as a predictive biomarker involved in immunotherapy response suppresses metastasis through EMT in colorectal cancer. Dis Markers. 2022;2022:9025668.
42. Asgari-Karchekani S, Karimian M, Mazoochi T, Taheri MA, Khamehchian T. CDX2 protein expression in colorectal cancer and itscorrelation with clinical and pathological characteristics, prognosis, and survival rate of patients. J Gastrointest Cancer. 2020;51:844–9.
43. Albuquerque C, Breukel C, van der Luijt R, Fidalgo P, Lage P, Slors FJ, et al. The 'just-right' signaling model: APC somatic mutations are selected based on a specific level of activation of the beta-catenin signaling cascade. Hum Mol Genet. 2002;11:1549–60.
44. Wu X, Luo F, Li J, Zhong X, Liu K. Tankyrase 1 inhibitior XAV939 increases chemosensitivity in colon cancer cell lines via inhibition of the Wnt signaling pathway. Int J Oncol. 2016;48:1333–40.
45. Chen B, Dodge ME, Tang W, Lu J, Ma Z, Fan CW, et al. Small molecule-mediated disruption of Wnt-dependent signaling in tissue regeneration and cancer. Nat Chem Biol. 2009;5:100–7.
46. Lau T, Chan E, Callow M, Waaler J, Boggs J, Blake RA, et al. A novel tankyrase small-molecule inhibitor suppresses APC mutation-driven colorectal tumor growth. Cancer Res. 2013;73:3132–44.
47. Tanaka N, Mashima T, Mizutani A, Sato A, Aoyama A, Gong B, et al. Mutations as a potential biomarker for sensitivity to tankyrase inhibitors in colorectal cancer. Mol Cancer Ther. 2017;16:752–62.
48. Verzi MP, Shin H, Ho LL, Liu XS, Shivdasani RA. Essential and redundant functions of caudal family proteins in activating adult intestinal genes. Mol Cell Biol. 2011;31:2026–39.
49. Simmini S, Bialecka M, Huch M, Kester L, van de Wetering M, Sato T, et al. Transformation of intestinal stem cells into gastric stem cells on loss of transcription factor Cdx2. Nat Commun. 2014;5:5728.
50. Guo RJ, Funakoshi S, Lee HH, Kong J, Lynch JP. The intestine-specific transcription factor Cdx2 inhibits beta-catenin/TCF transcriptional activity by disrupting the beta-catenin-TCF protein complex. Carcinogenesis 2010;31:159–66.
51. Bruun J, Sveen A, Barros R, Eide PW, Eilertsen I, Kolberg M, et al. Prognostic, predictive, and pharmacogenomic assessments of CDX2 refine stratification of colorectal cancer. Mol Oncol. 2018;12:1639–55.
52. Pilati C, Taieb J, Balogoun R, Marisa L, de Reyniès A, Laurent-Puig P. CDX2 prognostic value in stage II/III resected colon cancer is related to CMS classification. Ann Oncol. 2017;28:1032–5.
53. De Sousa E, Melo F, Wang X, Jansen M, Fessler E, Trinh A, et al. Poor-prognosis colon cancer is defined by a molecularly distinct subtype and develops from serrated precursor lesions. Nat Med. 2013;19:614–8.
54. Tomasello G, Barni S, Turati L, Ghidini M, Pezzica E, Passalacqua R, et al. Association of CDX2 expression with survival in early colorectal cancer: a systematic review and meta-analysis. Clin Colorectal Cancer. 2018;17:97–103.
55. Trinh A, Trumpi K, De Sousa E, Melo F, Wang X, de Jong JH, et al. Practical and robust identification of molecular subtypes in colorectal cancer by immunohistochemistry. Clin Cancer Res. 2017;23:387–98.
56. Robanus-Maandag EC, Koelink PJ, Breukel C, Salvatori DC, Jagmohan-Changur SC, Bosch CA, et al. A new conditional Apc-mutant mouse model for colorectal cancer. Carcinogenesis 2010;31:946–52.
57. van Neerven SM, Vermeulen L. The interplay between intrinsic and extrinsic Wnt signaling in controlling intestinal transformation. Differentiation 2019;108:17–23.
58. Fodde R. The APC gene in colorectal cancer. Eur J Cancer. 2002;38:867–71.
59. Zhao H, Ming T, Tang S, Ren S, Yang H, Liu M, et al. Wnt signaling in colorectal cancer: pathogenic role and therapeutic target. Mol Cancer. 2022;21:144.
60. de Sousa e Melo F, Kurtova AV, Harnoss JM, Kljavin N, Hoeck JD, Hung J, et al. A distinct role for Lgr5. Nature. 2017;543:676–80.
61. Michels BE, Mosa MH, Grebbin BM, Yepes D, Darvishi T, Hausmann J, et al. Human colon organoids reveal distinct physiologic and oncogenic Wnt responses. J Exp Med. 2019;216:704–20.

ACKNOWLEDGEMENTS

The results shown are in part based upon data generated by the TCGA Research Network: http://cancergenome.nih.gov/." Furthermore, we would like to express our gratitude to Jan Koster and the rest of the R2 team (AUMC) for raw data alignment and processing of the RNA sequencing data to the R2 platform. The flow cytometry facility at the Amsterdam University Medical Center (AUMC) for support with FACS sorting. Lisanne Nijman (AUMC) for technical support with the *Notum* and *Lgr5* scope. Alex Kirov for technical support with the organoid isolation. The mouse breeding facility and the core facility for genomics of the AUMC for their technical support. Finally, we would like to thank Nathalie Sphyris (CRUK Scotland Institute, Glasgow, UK) for critically reviewing this manuscript and Catherine Winchester for performing ImageTwin on the figures.

AUTHOR CONTRIBUTIONS

VW: conceptualization project, experimental design, in vitro organoid/tumoroid experiments, in vivo organoid/tumoroid experiments, analysis of mouse RNA sequencing datasets, data visualization, writing and original draft preparation. RH: in vivo organoid/tumoroid experiments. KC: in vitro organoid/tumoroid experiments. SH: processing and analysis of human datasets. AT: processing and analysis of human datasets. SB: genotyping. RJ and OS: providing KPN mouse model. SN: writing, original draft preparation and supervision. JM: conceptualization project, experimental design, writing, original draft preparation, supervision and funding acquisition. All authors have read and agreed to the published version of the manuscript.

COMPETING INTERESTS

The authors declare no competing interests.

ADDITIONAL INFORMATION

Supplementary information The online version contains supplementary material available at https://doi.org/10.1038/s41388-025-03365-5.

Correspondence and requests for materials should be addressed to Jan Paul Medema.